JACS
JOURNAL OF THE AMERICAN CHEMICAL SOCIETY

ARTICLE

pubs.acs.org/JACS

Nanoparticulate Pd Supported Catalysts: Size-Dependent Formation of Pd(I)/Pd(0) and Their Role in CO Elimination

Ana Iglesias-Juez,[†] Anna Kubacka,[†] Marcos Fernández-García,*[,†] Marco Di Michiel,[‡] and Mark A. Newton*[,‡]

[†]Instituto de Catálisis y Petroleoquímica, CSIC, C/Marie-Curie 2, 28049 Madrid, Spain

[‡]ESRF, 6, Rue Horowitz, BP-220, Grenoble F-38043, France

Supporting Information

ABSTRACT: A combination of time-resolved X-ray absorption spectroscopy (XAS), hard X-ray diffraction (HXRD), diffuse reflectance infrared spectroscopy (DRIFTS), and mass spectrometry (MS) reveals a series of size-dependent phenomena at Pd nanoparticles upon CO/(NO+O_2) cycling conditions. The multitechnique approach and analysis show that such size-dependent phenomena are critical for understanding Pd CO elimination behavior and, particularly, that different Pd(I) and Pd(0) centers act as active species for a size estimated by XAS to be, respectively, below and above ca. 3 nm. The relative catalytic performance of these two noble metal species indicates the intrinsic higher activity of the Pd(I) species.

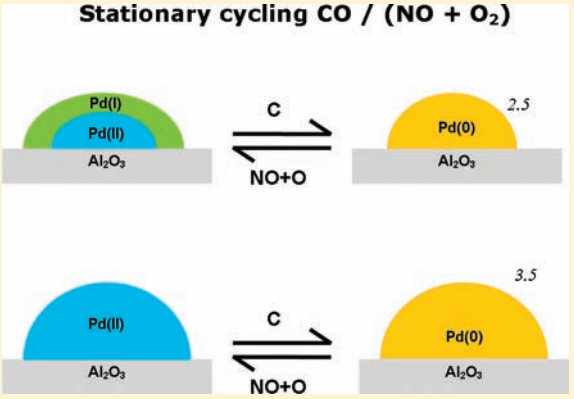

INTRODUCTION

Supported nanoparticulate Pd is the focus of research for application in a number of important areas. These include biomass conversion, coupling (e.g., Mizoroki−Heck and Suzuki−Miyaura, among others), and selective oxidation reactions for fine or high-value chemical(s) production, water gas shift, methane oxidation, and autoexhaust catalysis for pollution abatement.[1] Central to all these applications is the unique behavior of the noble metal in oxidation steps and/or processes. As such, a clear and fundamental comprehension of the nanoscale redox properties of Pd that underpin all these catalytic conversions is highly sought after.

Pd-based three way catalysts (TWCs) are a paradigmatic example of a technology for controlling pollutant emissions, specifically the removal of noxious NO_x emissions and the complete oxidation of hydrocarbons and CO to CO_2 in gasoline engine powered vehicles.[1g−j] Catalyst operation under light-off or isothermal conditions has been exhaustively evaluated,[1] but in recent years the focus has shifted to more realistic, dynamic, cyclic conditions.[2] Among the major issues targeted by early studies under cycling conditions, the key role of redox chemistry processes in controlling catalytic activity was clearly established.[2a,b,3] More recent studies have, however, revealed a significantly richer chemistry than may have been previously supposed. Particularly for CO elimination, there is intensive activity both at basic and at applied levels that indicates that CO oxidation can involve a series of unexpected steps. For CO/NO cycling conditions, a role for a Pd carbide phase resulting from CO dissociation has been recently demonstrated.[2e,f] Also, studies concerning the dynamics of the oscillatory catalytic behavior upon CO/O_2 mixtures have triggered a debate as to whether the most active phase relates to a surface Pd oxide layer[4] or is a metallic one dominated by chemisorbed oxygen.[5] All these studies confirm that Pd chemistry in pollutant elimination processes needs to be further clarified form a basic perspective.

To contribute to this end, we have analyzed CO elimination issues related to TWCs emissions using a "realistic" CO/(NO+O_2) mixture as a function of Pd nanoparticle size.[1,2] In this mixture, the two major oxidant species present in TW exhaust gases interact competitively for oxidizing the CO molecule. With this in mind, we analyze the behavior of two (2 and 4 wt %) Pd on alumina samples under operando, cycling conditions, using a multitechnique HXRD/XAS/DRIFTS/MS approach.[6] The synchronous use of a series of techniques providing bulk and surface as well as structural and electronic information allows us to extract conclusive evidence of a unique size-dependent chemistry in the Pd response to the reactive atmosphere.

EXPERIMENTAL SECTION

Two Pd/Al_2O_3 catalysts (with 2 and 4 wt % metal basis) were prepared by incipient wetness impregnation of a γ-Al_2O_3 support (supplied by Condea, S_{BET} = 200 m^2 g^{-1}) with aqueous solutions of $Pd(NO_3)_2 \cdot xH_2O$ (10 w/w %; Sigma Aldrich), followed by drying overnight at 383 K and calcination under air at 773 K for 2 h. Metal content (standard error ±3%) was checked using atomic absorption

Received: November 17, 2010
Published: March 03, 2011

dx.doi.org/10.1021/ja110320y | J. Am. Chem. Soc. 2011, 133, 4484–4489

spectroscopy. Samples are labeled as 2Pd and 4Pd according to their active metal content.

$CO/(NO+O_2)$ redox cycling experiments were carried out as previously described.[2d] The as-loaded sample was initially heated to 673 K in flowing He. Subsequently and holding the same temperature, two $CO/(NO+O_2)$ cycling experiments (each one having 10 repetitions of 13.65 × 2 s) were carried out over the sample, and HXRD/DRIFTS/MS (line ID15B; ESRF, Grenoble, France) or XAS/DRIFTS/MS (line ID24, ESRF, Grenoble, France) data were collected during each experiment. 5% CO and 5% ($NO+O_2$; 1:4.5) gas mixtures in He were used as reducing and oxidizing atmospheres, respectively. Gas flows were controlled with Bronkhorst mass flow controllers. All experimental data concern the second cycling experiment where pseudostationary conditions are reached.[2d] See the Supporting Information for additional information concerning the geometric details of the experimental setup.

Energy dispersive XAS measurements were carried out at the ID24 experimental station using a Si[311] Bragg polychromator and utilizing a FReLoN/CCD detector.[7] A spectral repetition rate of ca. 3 Hz spectrum was used. The resolution per pixel of the detector as used in these experiments is ca. 0.85 eV. The expected $\Delta E/E$ for ID24 is ca. 1×10^{-4}. Thus, an energy resolution for the dispersive XAS measurement at the Pd K edge of ca. 2.5 eV is realistic. A post factum measurement of the PdO and Pd foil reference compounds was also made after cooling under He to 300 K to serve as reference for fixing some degrees of freedom in the EXAFS analysis (see below).

XANES (X-ray absorption near edge structure) spectra were analyzed using the principal component analysis (PCA) methodology. PCA analysis assumes that a variable, in this case the absorbance in a set of spectra, can be mathematically modeled as a linear sum of individual, uncorrelated, components (known as factors) plus noise. An important property of this method is that each factor makes a maximum contribution to the sum of the variances of the variables; consequently, to determine the number of individual components, an F-test based on the variance associated with factor k and the summed variance associated with the pool of noise factors ($n-k$ factors, n being the total number of spectra) was performed. A factor was accepted as a "pure" chemical species (i.e., a factor associated with signal and not noise) when the percentage of significance level of the F-test, %SL, was lower than a test level, set in previous studies at 5%.[8] The latter means that the null hypothesis of the F test, for example, that factor k is associated with noise, is rejected for %SL values below such limiting value. The ratio between the reduced eigenvalues, REV, which describes the ratio between the mathematical norm of factors, was also used in determining the number of chemical species present in the sample. This ratio should approach one (e.g., equal statistical "weight") for noise-only factors. These tests are fully described in ref 8.

After identifying the number of principal components, it is necessary to transform the obtained abstract solution into the real components, that is, the solution with spectroscopic meaning. This can be done from two different initial situations. The first occurs when the principal components can be chemically identified by a target test (using external references corresponding to pure components). Suitable standard compounds are obviously necessary within this option. As detailed in the Supporting Information, the acute size/shape sensitivity of the XANES spectroscopy limits the viability of this option while working with nanoparticulate materials. A solution can still be found, even when the principal components have not been previously identified, by using iterative transformation factor analysis (ITFA), also known as self-modeling curve resolution.[8] In all procedures, the remaining problem is then to find the best transformation matrix, which rotates (through a nonorthogonal rotation) the abstract absorbance and concentration matrixes to an estimate of their real, physically meaningful forms. In the case of ITFA, a varimax rotation is previously performed in the abstract concentration matrix;[8a] this orthogonal rotation should align the abstract factors, as close as possible, along the unknown concentration profiles, revealing the reaction coordinate values (in our case, time under CO or $NO+O_2$ atmosphere) where the maximum concentration of each of the pure components would be observed. Uniqueness concentration vectors (TEST vectors having a unity value at a single reaction coordinate point) associated with these times are then subjected to testing and refinement by iteration. Each individual concentration profile is refined by setting to zero any emerging negative value. The iteration is stopped when the error in the test vector (RET) is lower than the real error (average statistical error obtained from PCA). The transformation matrix is then obtained for the concentration profiles, and a similar procedure is performed with the abstract spectrum matrix. The abstract solution is thus rotated, and XANES spectra and corresponding concentration profiles of the pure chemical components are obtained. Results in the main part of this Article are obtained through this second procedure.

Data reduction and analysis of the EXAFS (extended X-ray absorption fine structure) data was made using the EXCURV program.[9] Debye−Waller (DW) factors for the fitting of the fresh sample at room temperature were derived from fitting of Pd foil and PdO reference spectra obtained using conventional scanning EXAFS on XAS beamline BM29 at the ESRF. Goodness of fitting was measured through the R value: $R(\%) = (\int[\chi^T - \chi^E]k^3\,dk/[\chi^E]k^3\,dk) \times 100\%$, χ^T being the theoretically calculated EXAFS and χ^E being the EXAFS obtained via experiment.

HXRD measurements were carried out on ID15B (86.8 keV, λ = 0.143 Å, $\Delta E/E \approx 1.2 \times 10^{-3}$) using a digital flat-panel X-ray detector (Pixium 4700).[10] On ID15B the same sample environment employed at ID24 and described previously was used. HXRD patterns were recorded at 500 ms time resolution (2 Hz). Analysis of results using Rietveld subroutines was carried out using the XPert Highscore Plus (Panalytical) program.

DRIFTS measurements were made using a Bruker IFS 66 spectrometer and high sensitivity MCT detector. Infrared spectra were collected at a 3 Hz repetition rate and at 4 cm^{-1} resolution. Evolving gases analysis was carried out using a quadrupole mass spectrometer (Pfeiffer Omnistar).

RESULTS AND DISCUSSION

The complex chemistry of the Pd response to the dynamic $CO/(NO+O_2)$ conditions was first captured with XANES subjected to principal component analysis (PCA). PCA allows the determination of the number of noble metal chemical species involved in the reaction and the quantification of their corresponding evolution(s) throughout the reaction coordinate.[8]

The statistical tools described in the Experimental Section are applied in Tables 1 and 2 for the XANES spectra obtained, respectively, for our 2Pd and 4Pd samples. In both cases, we observed a sharp increase of %SL level between the second (4Pd; Table 2) or third (2Pd; Table 1) eigenvalue and the subsequent one. A similar behavior is observed for the REV ratio between eigenvalues. In the %SL case, this sharp increase coincides with the cutoff level of 5% typically admitted to differentiate between eigenvalues associated with signal and noise.[8] Thus, the presence of two and three palladium chemical species for, respectively, 4Pd and 2Pd, is demonstrated beyond doubt.

Figure 1 shows the concentration profiles (bottom) and XANES spectra corresponding to the pure chemical species (top) present during the treatment in stationary, cycling conditions. The XANES line shapes of the corresponding palladium chemical species show that both samples share two chemical species, presenting rather similar spectra between 2Pd and 4Pd, while an additional species is only detected in the 2Pd case. To assign such chemical species, Figure 2 displays the derivative

Table 1. Principal Component Analysis for the 2Pd Sample

n	eigenval	REV	variance	%SL
1	0.72665D+03	0.132×10^4	99.927	0.00
2	0.49476D+00	0.129×10^2	99.995	0.00
3	0.34037D−01	0.117×10^2	100.000	0.00
4	0.25524D−03	0.329×10^1	100.000	9.75
5	0.67225D−04	0.114×10^1	100.000	32.36
6	0.49845D−04	0.105×10^1	100.000	35.99
7	0.39166D−04	0.123×10^1	100.000	38.45
8	0.25159D−04	0.893	100.000	47.32
9	0.20895D−04	0.703	100.000	52.05
10	0.19601D−04	0.109×10^{-6}	100.000	56.76

Table 2. Principal Component Analysis for the 4Pd Sample

n	eigenval	REV	variance	%SL
1	0.61071D+03	0.169×10^4	99.946	0.00
2	0.32701D+00	0.258×10^4	100.000	0.00
3	0.11402D−03	0.128×10^1	100.000	16.72
4	0.79211D−04	0.204×10^1	100.000	17.62
5	0.34126D−04	0.132×10^1	100.000	32.79
6	0.22343D−04	0.920	100.000	40.74
7	0.20550D−04	0.108×10^1	100.000	40.79
8	0.15716D−04	0.886	100.000	45.77
9	0.14013D−04	0.811	100.000	47.77
10	0.12795D−04	0.810	100.000	49.77

spectrum of the three chemical species observed for 2Pd and the reference spectra of PdO and Pd bulk references. The derivative line shape is less sensitive to size/shape than is the XANES counterpart and can be used to visualize that two of the species display raising edges as well as shapes with marked similitude with the fcc Pd(0) foil and Pd(II):PdO (having the characteristic D_{2h}-like symmetry) reference compounds.[8b,d] The presence of Pd(0) is further corroborated by analysis of the EXAFS signal, which provides evidence of a Pd−Pd contribution at bonding distances characteristic of the metallic phase (ca. 2.75 Å; see EXAFS analysis section in the Supporting Information).

The third species (in red in Figures 1 and 2) has a more complex assignment; its derivative spectrum shows a raising edge close but shifted to higher energies with respect to the zerovalent reference and an intensity profile in the 24 350−24 380 eV region somewhat different from both Pd(0) and Pd(II) type species. The assignment of this species can be only carried out by careful study of the XANES line shape. The analysis of the main two continuum resonances (CRs) unveils the chemical nature of this component. First, the intensity of the CR at ca. 24 370 eV indicates a significant sp-electron deficiency with respect to a metallic (Pd(0)) state of the 2Pd sample (Figure 1) and thus a typical oxidic nature.[8b,d] Second, the intensity of the ca. 24 385 eV CR (assigned to the $l = 1$ projection of 4f Pd states) can be nevertheless associated to a certain metallic character, indicative of Pd−Pd contacts but at a larger distance (according to the $1/R^2$ rule) than that observed for Pd(0).[8b,d] The combination of these two pieces of information unequivocally indicates the presence of an oxidic species having a limited metallic character, as only observed in Pd(I) oxides having 1D or 2D like conduction.[11] To our knowledge, suitable reference XANES reference

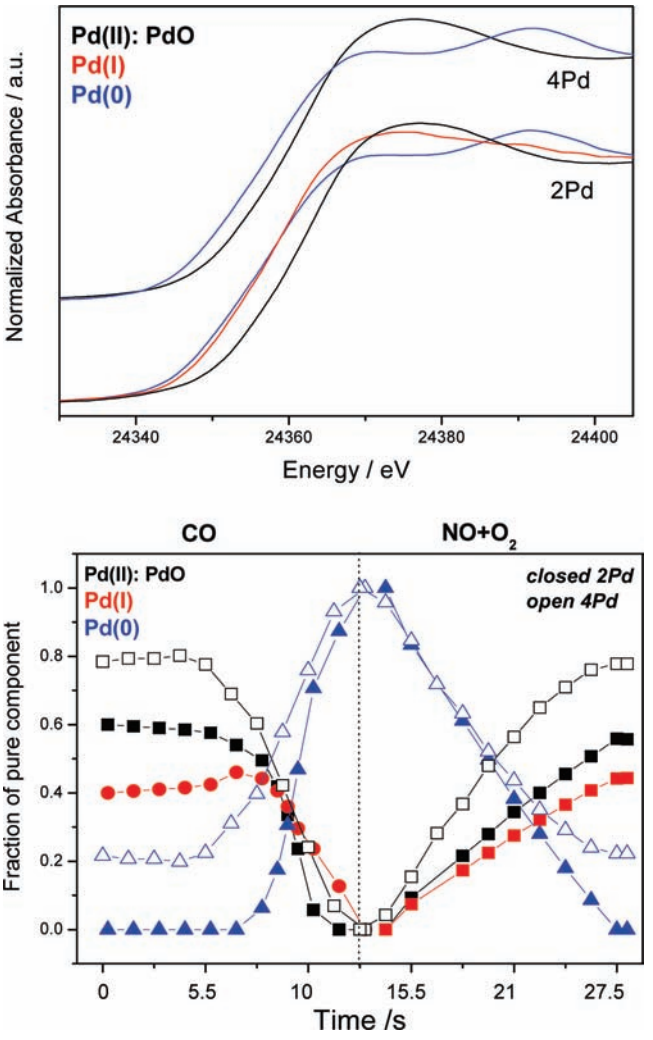

Figure 1. XANES spectra (top) and concentration profiles (bottom) corresponding to pure chemical species (obtained by PCA) present during a single CO/(NO+O_2) cycling treatment at 673 K.

measurements made on known Pd(I) oxide-type compounds are not available in the literature. As such, a further assessment of this assignment (from this perspective) is not currently possible. However, it is clear that the XANES line shape of this new species is significantly different from that expected from Pd metallic or Pd(II) oxidic species and, crucially, has characteristics that are consistent with those expected to arise from the electronic structure of a Pd(I) oxide.

The concentration profiles of the Pd chemical species present during the CO/(NO+O_2) cycling treatment show that the oxidized species are converted into the metallic Pd(0) one under the CO atmosphere, while the reverse process is observed upon a NO+O_2 atmosphere. Both XANES (Figure 1) and EXAFS (Figure 3; Pd−Pd vs Pd−O coordination numbers −CNs− for contributions at, respectively, first shell metallic or oxide phase coordination distances) give evidence of the exclusive presence of Pd(0) around the end of the CO step, while coexistence of oxidized and metallic species is observed in the complete NO+O_2 atmosphere and in a significant part of the CO step.

The apparent differences in the chemical behavior between both samples would therefore be most obviously related to the

dx.doi.org/10.1021/ja110320y |*J. Am. Chem. Soc.* 2011, 133, 4484–4489

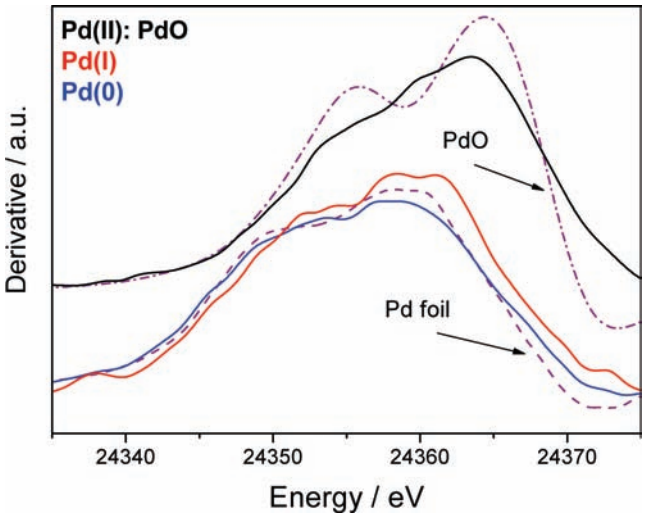

Figure 2. XANES derivative spectra of 2Pd pure chemical species (full lines) and PdO and Pd foil reference materials (discontinuous lines). For the sake of clarity, the Pd(II) species and PdO reference are vertically offset.

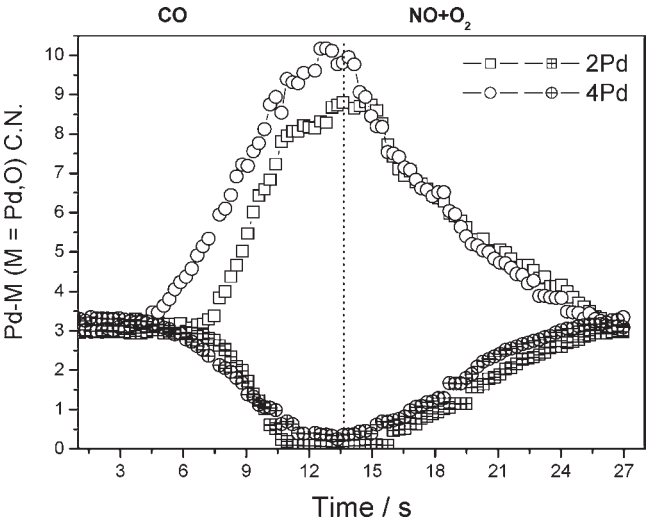

Figure 3. Pd−Pd (open symbols) and Pd−O (crossed symbols) EXAFS coordination numbers corresponding to metallic and oxidic first coordination shell, obtained during a single $CO/(NO+O_2)$ cycling treatment at 673 K. Standard error ±5%. See text for details.

presence of the Pd(I) species in 2Pd. In particular, the advent of this species in the 2Pd case delays the formation of Pd(0) under the CO atmosphere with respect to the 4Pd sample. Such differential behavior is confirmed using two additional techniques, EXAFS and HXRD. As mentioned, the correspondence between the Pd(0) temporal behavior from XANES (Figure 1) and EXAFS (Figure 3) is evident. From the CN obtained at the end of the CO treatment (8.4 ± 0.4 and 9.5 ± 0.5) and considering the fully reduced state reached at this point (as demonstrated by both XANES and EXAFS spectrocopies, Figures 1 and 3), we estimated an average 1.4 ± 0.2/2.5 ± 0.5 nm metallic size (i.e., diameter) for, respectively, 2Pd and 4Pd.[12] Note that EXAFS typically understimated size measurements by TEM; however, EXAFS allows in situ measurements in catalytic conditions and is thus used here to provide a dynamic track of the

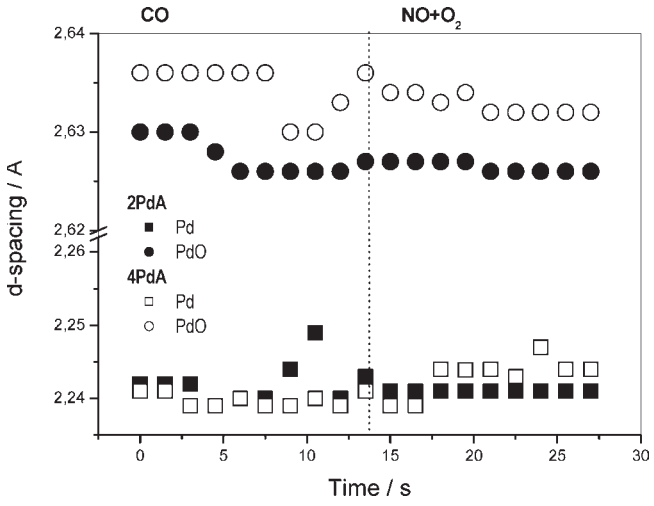

Figure 4. Peak position as a function of time for the Pd(111) and PdO(101) reflections during a single $CO/(NO+O_2)$ cycling treatment at 673 K. Standard error ±0.6%.

noble metal dimensionality. In our case, the EXAFS size understimation likely ranges from 1 to 2 nm.[13] A similar conclusion concerning the metallic appearance at different times for 2Pd and 4Pd can be extracted from HXRD. More importantly, HXRD adds new information related to the absence, in this case, of any obvious Pd carbide phase. As shown in Figure 4, maximum variation in metallic phase peak position(s) is ±0.05 Å, indicating that the Pd carbide phases, previously detected in ref 2e,2f for 2Pd and 4Pd upon CO/NO cycling conditions at 673 K, are very effectively suppressed in the current case (see the Supporting Information for further details concerning the $CO/(NO+O_2)$ vs CO/NO differential behavior as measured with HXRD).[2e,f]

To summarize, the structural XAS/HXRD characterization provided evidence of a differential behavior of the $Pd-Al_2O_3$ system as a function of noble metal particle size upon $CO/(NO+O_2)$ cycling conditions. For the 2Pd sample, which presents a fully developed (e.g., fully metallic) particle size of ca. 1.4 nm (end of CO step), we observed the presence of a partially oxidized Pd(I) species throughout the majority of the CO reducing step of the $CO/(NO+O_2)$ cycle, whose existence delays the appearance of the Pd(0) phase when compared to a 2.5 nm (4Pd case; end of CO step) particle (Figures 1 and 3). Again, we remark that particle sizes mentioned for the 2Pd/4Pd samples are obtained using EXAFS and typically underestimate the values obtained by TEM. Differences between EXAFS and other (TEM) techniques are crudely estimated in our case within an error of 1−2 nm; however, the magnitude of the EXAFS underestimation is, as already explained, size-dependent.[13] This fact would thus prohibit a more exact determination of the limit, although a lower value of 3 nm can be safely mentioned. The Pd(I) species would correspond to a surface oxide-containing layer or patch and has, as previously discussed, a distinctive electronic structure, which retains a certain metallic character. Note that such a layer/patch may contain the active species for CO oxidation recently mentioned by others in the case of CO/O_2 mixtures.[4] We however remark that the activity of oxidized Pd(II) species has been previously mentioned in the context of bulk or rather low dispersed surfaces/materials,[4] and, according to our data, such situation can differ markedly from the one characteristic of catalytic materials, with noble metal particle size typically below 5 nm.[1−3] Pd oxidation state differences at surface and inner

dx.doi.org/10.1021/ja110320y |J. Am. Chem. Soc. 2011, 133, 4484–4489

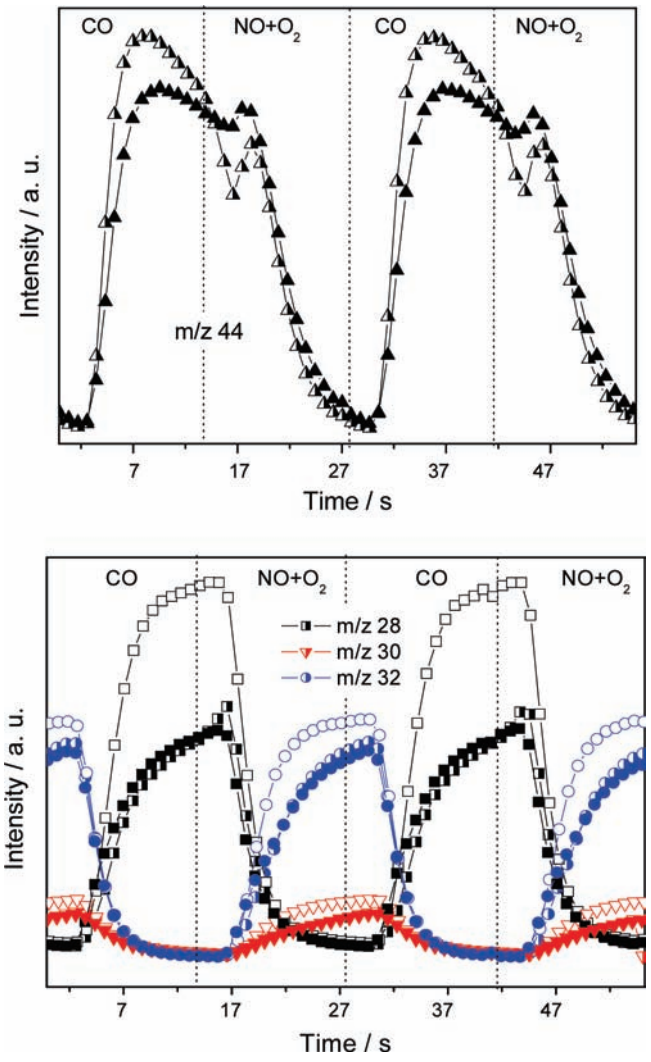

Figure 5. MS profiles for CO_2 (m/z 44; upper panel) and other reactant/products (lower panel) and production during CO/(NO+O_2) cycling treatment at 673 K. Open symbols. Al_2O_3; half-closed symbols. 2Pd; closed symbols. 4Pd. Squares, m/z 28; down-pointing triangles, m/z 30; circles, m/z 32; triangles, m/z 44.

(bulk) layers have been, on the other hand, previously described for prereduced catalysts using time-resolved EXAFS, but no detailed information was put forward to either identify the possible chemical origin of such differences or analyze a size-dependent behavior.[14] We further aimed to track this Pd(I) species while using the synchronously applied DRIFTS, but the weak nature of any Pd(I) carbonyls[15] prevents their detection under reaction conditions (DRIFTS results and a complete discussion of this last point are presented in the Supporting Information).

CO elimination products (e.g., CO_2) detected during the cycling treatment are depicted in Figure 5. Figure 5 also displays the time evolution of reactants, for example, CO (m/z 28), NO (m/z 30), and O_2 (m/z 32). The likely absence of N_2O (as measured using m/z 44 and 22 signals) indicates the NO elimination would generate exclusively N_2, which cannot be easily detected "in the presence" of CO using mass spectrometry as a result of a masking effect implicit in the relatively small amount of NO (and thus of N_2) present in the reactant mixture. In simple CO/NO mixtures, this was however easily detected at the same experimental conditions (e.g., temperature, cycling period, etc.) of this study.[2e,f]

As can be deduced from DRIFTS (see the Supporting Information), the onset of CO_2 formation in Figure 5 occurs when the CO molecule contacts the catalyst surfaces. However, at this particular time and according to XAS, the nature of the surface is very different in 2Pd and 4Pd samples. While using DRIFTS we are not able to calibrate the number of Pd(I) surface species, we can estimate that (according to EXAFS) the size difference between fully reduced catalysts (e.g., at the end of CO treatment) would indicate that 4Pd presents a metal surface area to the gas phase that is (at least) 30% larger than that provided by the 2Pd sample.[16] The normalized CO_2 production (using the surface areas of the 2Pd/4Pd metallic phases at the end of the CO step) profiles are presented in the Supporting Information. Taking into account the available noble metal surface area, we may conclude that while both Pd(I) and Pd(0) species are highly active species for CO elimination, the Pd(I) species formed only in the case of the 2Pd sample shows a superior performance for CO conversion.

We also note other size-dependent differences in behavior observed while the particles are fully metallic and concerning the fall off in in CO_2 production activity observed after the NO+O_2 step starting point (Figure 5). This drop is less drastic in 4Pd (with respect to 2Pd) and corresponds to a quicker CO stripping for the 4Pd surface as observed in the DRIFTS experiment (see Figure S6 in the Supporting Information). In agreement with O_2 consumption (Figure 5), the DRIFTS result indicates that O_2 interaction is favored as expected, for samples containing larger fractions of more closed metallic surfaces (Pd(111)-like ones characteristics of large particle size), and this in turn favors CO_2 production, according to the well-known "CO poisoning effect" observed in metallic surfaces.[2,5,17] Note that CO desorption can complicate this interpretation as it is size-dependent but only so weakly that no visible effect is expected in our experimental conditions (e.g., 2Pd vs 4Pd at 673 K).[17] On the other hand, the stronger interaction of O_2 (maybe in parallel with a lower interaction of the metal phase with the alumina support due to the size of the first component) may help in understanding the limited stability of Pd(I) species in the case of the 4Pd sample as compared to 2Pd.

CONCLUSIONS

The multitechnique XAS/HXRD/DRIFT/MS analysis of the Pd−Al_2O_3 system has revealed a series of size-dependent phenomena at Pd nanoparticles upon CO/(NO+O_2) cycling conditions. The most important is that both Pd(I) and Pd(0) species can be present in Pd surface layers, but this is strongly dependent on the size of the nanoparticles. Both species appear to be highly active species in CO elimination, but our results suggest a higher activity for the Pd(I) species. A Pd(I) chemical nature can be thus associated to the CO elimination "active" surface Pd oxide layers, at least in nanoparticulate materials below a size diameter, which can be roughly estimated to be around 3 nm. Above this size limit, we detected the exclusive presence of Pd(0) as active species for CO elimination at the surface of Pd nanoparticles. A potential instability of the Pd(I) species for noble metal particle sizes above 3 nm may be associated to a stronger interaction with the oxygen molecule with respect to particles with size below the

mentioned cutoff limit. These results would point to the ability to tune and maintain Pd nanoparticles of a certain size as being crucial to the most efficacious oxidation of CO during catalyst operation.

■ ASSOCIATED CONTENT

Supporting Information. Additional experimental details as well as XANES, EXAFS, HXRD, and DRIFTS data and analysis procedures. This material is available free of charge via the Internet at http://pubs.acs.org.

■ AUTHOR INFORMATION

Corresponding Author
mfg@icp.csic.es; newton@esrf.fr

■ ACKNOWLEDGMENT

We thank the ESRF for access to facilities (ID24, ID15b), Florian Perrin (ID24), and Anthony Mauro (ID15) for their technical assistance in making these measurements. A.K. and A.I.-J. thank MICINN for Ramón y Cajal postdoctoral grants.

■ REFERENCES

(1) (a) Vennestrom, P. R. N.; Christensen, C. H.; Pedersen, S.; Grundwaldt, J.-D.; Woodley, J. M. *ChemCatChem* **2010**, *2*, 249. (b) Karimi, B.; Behzadnia, H.; Elhamifar, D.; Akhavan, P. F.; Esfahani, F. K.; Zamani, A. *Synthesis* **2010**, *9*, 1399. (c) Lamblin, M.; Nassar-Hardy, L.; Hierso, J. C.; Fouquet, E.; Felpin, F.-X. *Adv. Synth. Catal.* **2010**, *352*, 33. (d) McGlaken, G. P.; Bateninn, L. M. *Chem. Soc. Rev.* **2009**, *38*, 2477. (e) Xué, L. Q.; Lin, Z. Y. *Chem. Soc. Rev.* **2010**, *39*, 1692. (f) Alonso, D. A.; Nájera, C. N. *Chem. Soc. Rev.* **2010**, *39*, 2891. (g) Twigg, M. V. *Appl. Catal., B* **2007**, *70*, 2.(h) Martínez-Arias, A.; Fernández-García, M.; Conesa, J. C.; Anderson, J. A. In *Supported Metal Catalysis*; Anderson, J. A., Fernández-García, M., Eds.; Imperial College Press: Singapore, 2005; Chapter 8. (i) Haaβ, F.; Fuess, H. *Adv. Eng. Mater.* **2005**, *7*, 899. (j) Trovarelli, A. *Catal. Rev.-Sci. Eng.* **1996**, *38*, 97.

(2) (a) González-Velasco, J. R.; Botas, J. A.; Farret, R.; González-Marcos, M. P.; Marc, J. L.; Gutiérrez-Ortiz, M. A. *Catal. Today* **2000**, *59*, 395. (b) Wu, X.; Wand, D. *Appl. Surf. Sci.* **2004**, *221*, 375. (c) Newton, M. A.; Belver-Coldeira, C.; Martínez-Arias, A.; Fernández-García, M. *Nat. Mater.* **2007**, *6*, 528. (d) Newton, M. A.; Belver-Coldeira, C.; Martínez-Arias, A.; Fernández-García, M. *Angew. Chem., Int. Ed.* **2007**, *46*, 8629. (e) Newton, M. A.; Di Michiel, M.; Kubacka, A.; Fernández-García, M. *J. Am. Chem. Soc.* **2010**, *132*, 4540. (f) Kubacka, A.; Martínez-Arias, A.; Fernández-García, M.; Di Michiel, M.; Newton, M. A. *J. Catal.* **2010**, *270*, 275. (g) Wang, Q.; Zhao, B.; Zhou, R. *Environ. Sci. Technol.* **2010**, *44*, 3870.

(3) Iglesias-Juez, A.; Newton, M. A.; Fiddy, S. G.; Martínez-Arias, A.; Fernández-García, M. *Chem. Commun.* **2005**, 4052.

(4) (a) Hendriken, B. L. H.; Bobaru, S. C.; Frenken, J. W. M. *Top. Catal.* **2005**, *36*, 43. (b) Hendriken, B. L. H.; Ackermann, M. D.; van Rijn, R.; Stolz, D.; Popa, I.; Balmes, O.; Resta, A.; Werneille, D.; Felici, R.; Ferrer, S.; Frenken, J. W. M. *Nat. Chem.* **2010**, *2*, 730. (c) van Rijn, R.; Balmes, O.; Felici, R.; Gustafson, J.; Wermeille, D.; Westerton, R.; Lundgren, E.; Frenken, J. W. M. *J. Phys. Chem. C* **2010**, *114*, 6875.

(5) (a) Gao, F.; Wang, Y.; Goodman, D. W. *J. Phys. Chem. C* **2009**, *113*, 174. (b) Gao, F.; Cai, Y.; Gath, K. K.; Wang, Y.; Chen, M. S.; Guo, Q. L.; Goodman, D. W. *J. Phys. Chem. C* **2009**, *113*, 182. (c) McClure, J.; Goodman, D. W. *Chem. Phys. Lett.* **2009**, *469*, 1.

(6) (a) Weckhuysen, B. M. *Angew. Chem., Int. Ed.* **2009**, *48*, 4910. (b) Tinnemans, S. J.; Mesu, J. G.; Kervinen, K.; Visser, T.; Nijhuis, T. A.; Beale, A. M.; Keller, D. E.; van der Eerden, A. M. J.; Weckhuysen, B. M. *Catal. Today* **2006**, *113*, 3.

(7) Labiche, J.-C.; Mathon, O.; Pascarelli, S.; Newton, M. A.; Guilera Ferre, G.; Cuifs, G.; Vaughan, G.; Homs, A.; Fernandez Carreiras, D. *Rev. Sci. Instrum.* **2007**, *78*, 091301.

(8) (a) Fernández-García, M.; Márquez, C.; Haller, G. L. *J. Phys. Chem.* **1995**, *99*, 12565. (b) Fernández-García, M. *Catal. Rev.-Sci. Eng.* **2002**, *44*, 52.(c) Malinoswky, E. R. *Factor Analysis in Chemistry*; Wiley: New York, 2002. (d) Fernández-García, M.; Iglesias-Juez; Martínez-Arias, A.; Hungría, A. B.; Anderson, J. A.; Conesa, J. C.; Soria, J. *J. Catal.* **2004**, *221*, 594.

(9) Binsted, N. *EXCURV, CCLRC Daresbury Laboratory computer programme*, 1998.

(10) Daniels, J. E.; Drakopoulos, M. *J. Synchrotron Radiat.* **2009**, *16*, 463.

(11) Shannon, R. D.; Rogers, D. B. *Inorg. Chem.* **1971**, *10*, 713.

(12) (a) Agostini, G.; Pellegrini, R.; Leofanti, G.; Birtinetti, L.; Bertarione, S.; Groppo, A.; Lamberti, C. *J. Phys. Chem. C* **2009**, *113*, 10485. (b) Jentys, A. *Phys. Chem. Chem. Phys.* **1999**, *1*, 4059.

(13) A note can be added in comparing particle size measured with EXAFS and the more usual TEM technique. We have previously made comparisons during similar (to current ones) CO/NO cycling treatments and found that EXAFS estimation of the particle size can be significantly smaller with respect to those obtained using TEM. TEM yields average particle size estimations of 2.5−3 nm for the 2Pd sample and 3.5−4 nm for the 4Pd case (see ref 2f for further details). However, trends as a function of the Pd loading would be roughly consistent among both techniques if we consider that metal particles below 1 nm likely escape TEM detection. This fact, on the other hand, infers that the difference between EXAFS and TEM measurements has an inherent size-dependence in the size range explored in this work. HXRD may generate an additional estimation of primary particle size. In this case, due to the dynamic, high temperature, in operando experimental conditions, we were unable to adequately handle strain and/or the influence of absorbates in size measurements using either the width and/or the position (*d*-spacing) of HXRD peaks.

(14) (a) Matsuma, D.; Okajima, Y.; Nishihata, Y.; Mizuki, J.; Taniguchi, M.; Uenishi, M.; Tanaka, H. *J. Phys.: Conf. Ser.* **2009**, *190*, 012154. (b) Matsuma, D.; Nishihata, Y.; Mizuki, J.; Taniguchi, M.; Uenishi, M.; Tanaka, H. *J. Appl. Phys.* **2010**, *107*, 124319.

(15) (a) Bensalem, A.; Muller, J. E.; Tessier, D.; Bozon-Verduraz, F. *J. Chem. Soc., Faraday Soc.* **1996**, *92*, 3233. (b) Iglesias-Juez, A.; Martínez-Arias, A.; Fernández-García, M. *J. Catal.* **2004**, *221*, 148. (c) Lamberti, C.; Zecchina, A.; Groppo, E.; Bordiga, S. *Chem. Soc. Rev.* **2010**, *39*, 4951.

(16) EXAFS particle size allows an estimation (according to procedures thoroughly described in ref 12 and as it has been exemplified in ref 2f) of the metal dispersion, being 70%/46% for, respectively, 2Pd/4Pd samples. If we arbitrarily add 1 nm to the sizes measured by EXAFS to roughly account for the technique underestimation of the observable, we found a 48%/35% dispersion for, respectively, 2Pd/4Pd samples. Considering the metal loading of each sample, these values give the mentioned difference of ca. 30% (EXAFS size) or 45% (EXAFS size plus 1nm) in (gas phase) available noble metal surface area. So, an estimation of a 30% difference seems conservative for our purposes.

(17) (a) Libuda, J.; Freund, H.-J. *Surf. Sci. Rep.* **2005**, *57*, 157. (b) Schalow, T.; Brandt, B.; Starr, D. E.; Laurin, M.; Shaikhtudinov, S. K.; Schauermann, S.; Libuda, J.; Freund, H.-J. *Phys. Chem. Chem. Phys.* **2007**, *9*, 1347.